CO_2 Methanation Reaction Pathways over Unpromoted and $NaNO_3$-Promoted Ru/Al_2O_3 Catalysts

Sang Jae Park,[1] Xiang Wang,[2] Madelyn R. Ball,[1] Laura Proano,[1] Zili Wu,[2] Christopher W. Jones[1]*

[1]School of Chemical & Biomolecular Engineering, Georgia Institute of Technology, 311 Ferst Dr., Atlanta, GA 30332, USA

[2]Chemical Science Division, Oak Ridge National Laboratory, 1 Bethel Valley Road, Oak Ridge, TN 37831, USA

*Email: cjones@chbe.gatech.edu

Abstract

Catalytic CO_2 sorbents, materials that adsorb and pre-concentrate CO_2 on the catalyst surface prior to subsequent conversion, are becoming important materials in CO_2 capture and utilization. In this work, a prototypical CO_2 methanation catalyst - Ru/Al_2O_3 - and a related catalytic sorbent - $NaNO_3/Ru/Al_2O_3$ – are used for CO_2 methanation in flowing hydrogen in a fixed bed reactor at temperatures ranging from 220 to 280 °C. Activation energies for the $NaNO_3/Ru/Al_2O_3$ material are slightly higher than unpromoted Ru/Al_2O_3 catalysts, and the reaction orders vary more significantly. *In situ* IR spectroscopy and steady-state isotopic kinetic analysis (SSITKA) using *in situ* IR/MS spectroscopy show that bicarbonate and linear carbonyl species are the likely reaction intermediates over unpromoted Ru/Al_2O_3, while bidentate carbonate, formate and linear carbonyl species are among likely reaction intermediates over $NaNO_3/Ru/Al_2O_3$. Rate laws consistent with the obtained experimental data are proposed after kinetic modeling of multiple plausible reaction pathways. Results suggest that the pathway over the $NaNO_3/Ru/Al_2O_3$ catalyst likely has an additional kinetically relevant irreversible step in the CO_2 methanation reaction pathway.

Keywords: catalytic sorbent, DFM, CCUS, carbon dioxide

1. Introduction

Global atmospheric carbon dioxide levels have increased throughout the last century, and CO_2 has been reported to be one of main contributors to climate change, necessitating emissions reductions and CO_2 sequestration and utilization.[1–3] Among different products that can be easily produced from CO_2, methane production via hydrogenation of CO_2 is attractive, as there is already existing infrastructure for transport and storage of natural gas. The reaction between CO_2 and H_2 to produce CH_4, also known as the Sabatier reaction, is thermodynamically favorable, with ΔG_{298K} = -113 kJ/mol. Catalytic methanation of CO_2 is typically performed between 200 °C ~ 450 °C at atmospheric pressure, mild conditions compared to the production of other higher hydrocarbons or oxygenates.[4,5] Over the years, numerous studies have been conducted on CO_2 methanation using different supported metal catalysts, including Fe, Ni, Pd, Ru, and Rh.[6–9] In particular, supported ruthenium has been reported as the catalyst with the highest selectivity towards methane.

There have been numerous studies regarding CO_2 methanation mechanisms over ruthenium supported on different oxide supports (i.e. Al_2O_3, TiO_2, CeO_2), and it is widely accepted that CO_2 methanation occurs through a carbonyl intermediate (CO*). However, there is still not a consensus regarding how the carbonyl species are formed. Two general schemes have been proposed in the literature. In one scheme, CO_2 dissociates to adsorbed CO* and O* species, and CO* reacts with surface hydrogen to form methane. In the other proposed scheme, CO* is formed through the reverse water gas shift reaction (RWGS) via formate species (HCOO*) as an intermediate.

Many reports describe the synthesis of supported ruthenium catalysts with improved activity and selectivity via inclusion of different additives or promoters, and several studies reported that alkali (Na, K, Li)[10–14] or alkaline earth metals (Mg, Ca, Ba)[15–19] provide improved performance. For example, Li et al. reported that alkali nitrate promoted Ru/Al_2O_3 gave up to three times higher

methane production rates compared to unpromoted Ru/Al_2O_3. The improvement in methanation activity was attributed to modification of the local electron density of Ru and removal of depositional inactive carbon by alkaline carbonate catalysis. Panagogiotopoulou et al. also reported that alkali metal ion (e.g. K, Li, or Na) loaded Ru/TiO_2 showed higher conversion of CO_2 than catalysts without additives, while still showing higher selectivity toward methane, between temperatures of 200 °C and 450 °C. However, the reaction pathway toward CH_4 formation over such alkali promoted ruthenium catalysts, whether similar or different to unpromoted ruthenium catalysts, remains unclear.

Furthermore, there is growing interest in utilizing ruthenium catalysts and alkali metal promoted sorbents to synthesize dual function materials (DFM) or catalytic sorbents for integrated capture and methanation of CO_2.[20–27] Alkali salts can enhance the sorption of CO_2 under reaction conditions, changing the surface coverages of the catalysts. To this end, we seek to develop a thorough understanding of CO_2 methanation mechanism(s) over alkali promoted ruthenium catalysts, with this understanding being crucial for designing effective DFMs/catalytic sorbents.

In our previous work, an initial assessment of possible reaction pathways over Ru/Al_2O_3 and $NaNO_3/Ru/Al_2O_3$ was presented backed by kinetic measurements and observations through *in situ* FTIR during CO_2 methanation reaction conditions.[24] However, operando experiments were not yet performed in the previous work, and in the absence of such experiments, it was difficult to distinguish true reaction intermediates from spectator species. In the present work, CO_2 methanation reaction pathways over Ru/Al_2O_3 and $NaNO_3/Ru/Al_2O_3$ catalysts, with the former catalyst a well-studied model system and the latter a candidate DFM. Kinetic measurements, identifying apparent H_2 and CO_2 reaction orders, along with apparent activation energies, are measured over the different catalysts. The catalysts are further characterized through

chemisorption experiments and transmission electron microscopy (TEM), while reaction pathways are studied through *in situ* DRIFTS measurements during the CO_2 methanation reaction, as well as steady state isotopic transient kinetic experiments utilizing $^{12}CO_2$ and $^{13}CO_2$ feeds. Plausible reaction pathways consistent with experimental data are proposed and further investigated by kinetic modeling to obtain the most representative reaction pathways over different catalysts.

2. Experimental Section

2.1. Synthesis of Ru/Al_2O_3 and $NaNO_3/Ru/Al_2O_3$ catalysts

To synthesize 1% and 5% Ru/Al_2O_3 catalysts, a predetermined amount of ruthenium (III) nitrosyl nitrate ($Ru(NO)_3(NO_3)_3$, Alfa Aesar) was dissolved in distilled water to obtain stock solutions of different concentrations. Using incipient wetness impregnation, the prepared solution was added to γ-Al_2O_3 (Sasol). After impregnation, the samples were first dried at 100 °C for 4 h then calcined at 450 °C for 2 h in 21% O_2/He (flow rate =100 mL/min). The temperature ramp was 5 °C/min. Sodium nitrate addition to synthesize 5% $NaNO_3$/1% Ru/Al_2O_3 and 5% $NaNO_3$/5% Ru/Al_2O_3 catalysts was performed by incipient wetness impregnation of $NaNO_3$ (sigma Aldrich), using distilled water as solvent, to the calcined 1% Ru/Al_2O_3 and 5% Ru/Al_2O_3 catalysts. Then the samples were calcined at 350 °C in static air for 30 min.

2.2. Characterization

2.2.1. Transmission electron microscopy

Scanning transmission electron microscopy (STEM) images were collected on an HD 2700 Hitatchi aberration corrected STEM. Catalyst samples dispersed in acetone were dropped on holey carbon coated Cu grids.

2.2.2. CO Chemisorption

Pulse CO chemisorption were performed using a Micromeritics AutoChem II 2920. Approximately 50 mg of samples were loaded into a U-shape quartz tube on a bed of quartz wool. The samples were then heated 350 °C and held for 1 h under 10% H_2/He flow. Heating ramp of 5 °C/min was used. The gas was then switched to He flow for 30 min to remove any adsorbed species. The temperature was then lowered to 30 °C, which was followed by CO pulse testing. Doses of 10% CO/He were flowed through the sample bed and analyzed by thermal conductivity detector. After saturation with CO was reached, He passed through the sample bed for 60 min. A stoichiometry of Ru/CO = 1.667 was used to calculate metal dispersion.[28,29]

2.3. Reaction Measurements

The catalytic reactions were performed in a stainless-steel tube reactor with inner diameter of ¼" at a total pressure of 1 atm. The stainless-steel tube was placed inside an electric furnace, and a K-type thermocouple was used for temperature control. All catalysts were first pressed at 1000 psi to form pellets, and then crushed and sieved between 125 and 425 microns in size, and for each experiment 20~30 mg of sieved catalysts were used. A gas hourly space velocity of 38400~57600 mL g^{-1} h^{-1} was used. In a typical experiment, the samples were reduced at 350 °C for 1 h in 10% H_2/N_2 at 20 mL/min. After the reduction step, temperature was cooled to 260 °C. Then the feed containing 10~40% of CO_2 and 20~50% H_2, and balance N_2 was used to for reactions, including reaction order measurements. Total flow was always kept constant at 20 mL/min. The apparent activation energy was also determined by measuring the methane production rate at varying reaction conditions between 220 °C and 280 °C. Calculations to ensure the mass transfer limitations are negligible and that the kinetic measurements are far from equilibrium were performed, as shown in Supplementary Information (Sections IV and V).

2.4. In situ DRIFTS experiments

In situ diffuse reflectance infrared Fourier transform spectroscopic (DRIFTS) experiments were performed using a Harrick Praying Mantis high-temperature reaction chamber with ZnSe window to observe surface species on the catalysts during the CO_2 methanation reaction. The spectrometer used for the experiments was a Thermo Nicolet iS10 IR spectrometer with a mercury cadmium telluride (MCT) detector. Samples were initially pretreated under 10% H_2/N_2 at 40 mL/min at a temperature of 350 °C for 1 h. The temperature was then lowered to 50 °C, and a background scan was taken under He flow. Then a flow of 5% CO_2/20% H_2/N_2 at 40 mL/min flowrate was passed through the cell, and a scan was taken at temperatures of 50 °C, 100 °C, 200 °C, and 300 °C.

2.5. Steady State Isotopic Transient Kinetic Analysis

For the surface species observed during the CO_2 methanation reaction, to distinguish reaction intermediates from spectator species on the different catalysts, steady state isotopic transient kinetic analysis (SSITKA) combined with DRIFTs (on a Bruker Tensor 27 FTIR spectrometer with an MCT detector) experiments were performed. In a typical experiment, samples were pretreated under 10% H_2/N_2 at 40 mL/min at temperature of 300 °C for 1 h. The temperature was then lowered to 260 °C, and a background scan was taken at He flow. Then a flow of 5% $^{12}CO_2$/20% H_2/N_2 at 40 mL/min flowrate was flowed into the DRIFTS Praying Mantis high temperature cell from Harrick. Once the steady state was reached, the flow was switched to 5% $^{13}CO_2$/20% H_2/N_2 at 40 mL/min. The change in intensity of $^{12}CO_2/^{13}CO_2$ related surface species observed through DRIFT spectra and the concentration of $^{16}CH_4/^{17}CH_4$ in the cell outlet measured by a mass spectrometer (OmniStar from Pfeiffer Vacuum) were analyzed to identify kinetically relevant reaction intermediates. To check whether the experimentally observed shift

that occurred upon switching from $^{12}CO_2$ to $^{13}CO_2$ flow fit the theoretical shift for each surface species, Eq. (1) and Eq. (2) were used, where wavelength is represented by ν, and reduced mass is represented by μ, while the mass of each atom is represented by m_A or m_B.

$$\frac{\nu_{C^{13}}}{\nu_{C^{12}}} = \sqrt{\frac{\mu_{C^{12}}}{\mu_{C^{13}}}} \qquad \text{Eq. (1)}$$

$$\mu = \frac{m_A m_B}{m_A + m_B} \qquad \text{Eq. (2)}$$

2.6. Kinetic Modeling

Based on results from *in situ* IR and SSITKA/DRIFTs experiments, multiple different reaction pathways that fit spectroscopic observations were proposed, and rate laws that correspond to proposed reaction sequences were derived. Regression of experimental data to obtained rate laws was performed using Microsoft Excel solver with the GRG nonlinear engine for nonlinear functions. The rate constants and equilibrium constants were fitted using the least mean squares method, and the uncertainties of kinetic parameters were quantified using the Jackknife resampling method.[30]

3. Result and Discussion

3.1. Characterization

Particle size distribution analysis from TEM images and CO chemisorption experiments was performed to obtain metal dispersion of synthesized catalysts, as shown in Table 1. It should be noted that the metal dispersions obtained from CO chemisorption were typically higher than those obtained from those obtained from analysis of TEM images. This is likely because there was an overestimation of surface ruthenium sites, as a stoichiometry of Ru/CO = 1.667 was used. Stoichiometries for Ru/CO between 1.5 and 2 have been commonly used to estimate ruthenium dispersion, as it has previously been reported that bridging carbonyls are more dominant than linear

or dicarbonyl species.[28,29,31] However, CO chemisorption has been reported to be dependent on the particle size of Ru, with dicarbonyl or tricarbonyl becoming more important for smaller particle sizes. The synthesized catalysts in our work had quite broad particle size distributions, as shown in **Figure S1**, potentially making it difficult to obtain accurate dispersion values from CO chemisorption. Therefore, in calculations of turnover frequency, dispersions obtained from analysis of TEM images were used. It should be noted that if a stoichiometry of Ru/CO=1 is used, the metal dispersion from CO chemisorption corresponds well to the dispersion data obtained from TEM analysis, as shown in **Table 1**. Catalysts of 1% metal loading and 5% metal loading had similar average particle sizes, with metal dispersions of 9.1% and 9.3% observed from the TEM analysis. $NaNO_3$ loaded catalysts showed decreased metal dispersions of 6.4% and 6.6%, for 1% and 5% metal loadings, respectively. Similar to the unpromoted catalysts, there were not significant differences in the metal dispersion between the two loadings.

Table 1. Metal dispersion of catalysts measured by CO chemisorption and TEM particle size distribution analysis. For averaging particle sizes measured by TEM, at least 240 particles were used for all catalysts. For metal dispersion by CO chemisorption, Ru/CO = 1.667 was assumed.

	Average particle size – TEM analysis (nm)	Metal dispersion - TEM analysis (%)	Metal dispersion – CO chemisorption (%)
1% Ru/Al_2O_3	12.1 ± 6.9	9.1	15.5
5% Ru/Al_2O_3	11.6 ± 5.7	9.3	14.4
$NaNO_3$/1% Ru/Al_2O_3	17.3 ± 10.9	6.4	8.9
$NaNO_3$/5% Ru/Al_2O_3	16.6 ± 9.4	6.6	7.7

3.2. *Kinetic Measurements*

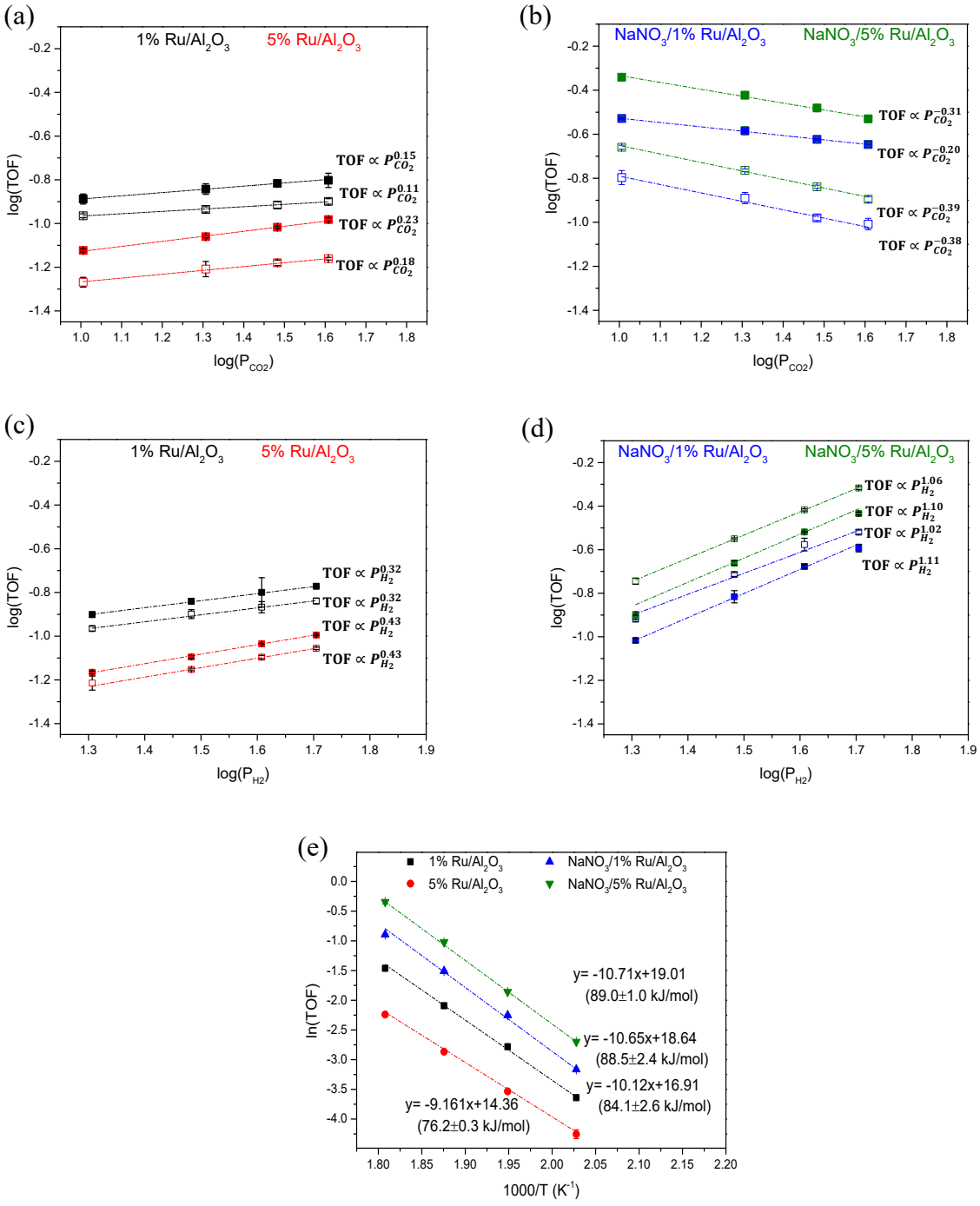

Figure 1. CO_2 reaction order for (a) Ru/Al_2O_3 catalysts and (b) $NaNO_3/Ru/Al_2O_3$ catalysts (filled points = 40% H_2 and hollow points = 20% H_2), and H_2 reaction order for (c) Ru/Al_2O_3 catalysts and (d) $NaNO_3/Ru/Al_2O_3$ catalysts (filled points = 40% CO_2 and hollow points = 20% CO_2) measured at 260 °C. (e) Arrhenius plot for CO_2 methanation in the temperature range between 220 °C and 280 °C for both Ru/Al_2O_3 and $NaNO_3/Ru/Al_2O_3$ catalysts.

Figure 1 (a) and (b) show the dependence of the CH_4 formation rate on the CO_2 partial pressure over different catalysts. For 1% Ru/Al_2O_3, CO_2 reaction orders of 0.15 (40% H_2) and 0.11 (20% H_2) were observed, while 5% Ru/Al_2O_3 showed CO_2 reaction orders of 0.23 (40% H_2) and 0.18 (20% H_2). For $NaNO_3$/1% Ru/Al_2O_3, CO_2 reaction orders of -0.20 (40% H_2) and -0.38 (20% H_2) were observed, while $NaNO_3$/5% Ru/Al_2O_3 showed CO_2 reaction orders of -0.31 (40% H_2) and -0.39 (20% H_2). Negative CO_2 reaction orders for the $NaNO_3$ loaded samples imply that addition of $NaNO_3$ to Ru/Al_2O_3 gave increased surface coverage of either CO_2 or CO_2-derived species on the catalyst surface. It was previously reported that molten alkali metal ions can dissolve CO_2 under similar conditions.[32–35] For all four samples, CO_2 reaction orders were larger at higher H_2 partial pressures. This can be attributed to competitive adsorption between H_2 and CO_2, with the increase in the H_2 partial pressure leading to a higher surface coverage of H* species, which causes a decrease in the surface coverage of CO_2-related reaction intermediates, leading to increased CO_2 reaction orders.

Figure 1 (c) and (d) shows the dependence of the CH_4 formation rate on the H_2 partial pressure over different catalysts. For, 1% Ru/Al_2O_3, H_2 reaction orders of 0.32 was observed, while 5% Ru/Al_2O_3 showed H_2 reaction orders of 0.43. For the sodium nitrate promoted samples, $NaNO_3$/1% Ru/Al_2O_3 showed H_2 reaction orders of 1.11 (40% CO_2) and 1.02 (20% CO_2), while $NaNO_3$/5% Ru/Al_2O_3 showed H_2 reaction orders of 1.10 (40% CO_2) and 1.06 (20% CO_2). Regardless of the loading of ruthenium, addition of $NaNO_3$ caused a significant increase in the H_2 reaction order, leading to decreased H surface coverage. It should be noted that the observed H_2 reaction orders for $NaNO_3$ loaded catalysts are much higher than those values previously reported for supported ruthenium catalysts. Prairie et al. reported a H_2 reaction order of 0.57 over Ru/TiO_2 at 110 °C, while Szanyi et al. reported H_2 reaction orders between 0.3 and 0.5 over different

Ru/Al_2O_3 catalysts at reaction temperatures between 240 °C and 300 °C.[31,37] Farrauto et al. reported a slightly higher order of 0.88 over a Ru/Al_2O_3 catalyst at a temperature of 230 °C.[22] Previous studies that reported similar H_2 reaction order measurements over other noble metals, such as Pd or Rh, also noted orders between 0.5 and 0.8.[37,38] While dissociation of the C-O bond of carbonyl species with assistance of surface H* species is considered as a consensus rate determining step in the CO_2 methanation reaction in supported ruthenium catalysts, the high H_2 reaction order observed for $NaNO_3$ loaded Ru/Al_2O_3 catalysts indicates that $NaNO_3$ loaded Ru/Al_2O_3 catalysts may have different or additional kinetically relevant step(s) to Ru/Al_2O_3 catalysts. Similar to what was observed for the CO_2 reaction orders, H_2 reaction orders were also higher with higher partial pressures of CO_2.

Figure 1 (e) shows the apparent activation energy of the CO_2 methanation reaction over different catalysts under $10\%CO_2/40\%H_2/N_2$ flow. Apparent activation energies of 82 and 76 kJ/mol were observed for 1% Ru/Al_2O_3 and 5% Ru/Al_2O_3. The obtained activation energies aligns with previously reported values for supported ruthenium catalysts. For instance, Prairie et al. reported an apparent activation energy of 79 kJ/mol over Ru/Al_2O_3 catalysts, and Szanyi et al. reported activation energies between 65 kJ/mol and 80 kJ/mol over different metal loadings of Ru/Al_2O_3 catalysts.[31,36,39] Upon addition of $NaNO_3$, both promoted catalysts here showed an increase in the apparent activation energy, with values of 86 and 90 kJ/mol for $NaNO_3$/1% Ru/Al_2O_3 and $NaNO_3$/5% Ru/Al_2O_3, respectively. The observed increase in the activation energy upon addition of $NaNO_3$ agrees well with previously reported alkali salt promoted ruthenium catalysts, as well as to our previous work for $NaNO_3/1\%Ru/Al_2O_3$.[13,24] In our previous work, it was hypothesized that the two catalysts may have a similar rate determining step, due to relatively small differences in the apparent activation energies between 1% Ru/Al_2O_3 and $NaNO_3$/1%

Ru/Al_2O_3. However, the differences in the apparent activation energies for 5% Ru/Al_2O_3 and $NaNO_3$/5% Ru/Al_2O_3 were more significant than at 1% Ru loading, as observed in **Figure 1 (e)**. Based on these observations, we considered whether there may be a change in the rate determining step, or inclusion of additional kinetically relevant steps for the $NaNO_3/Ru/Al_2O_3$ catalysts, which is further discussed alongside the kinetic modelling of different reaction pathways below (section 3.5).

3.3. In-situ DRIFTS measurements

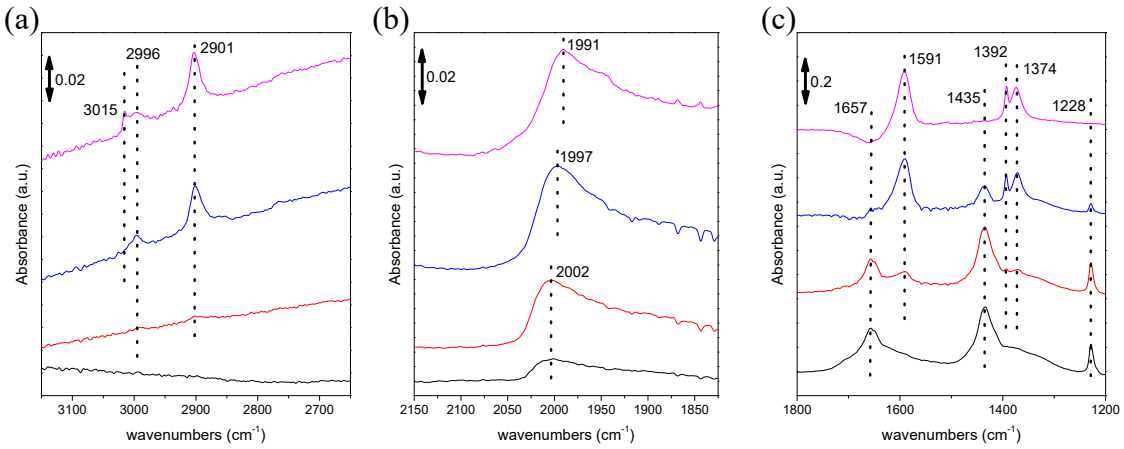

Figure 2. DRIFT spectra taken over 5% Ru/Al_2O_3 under 5%CO_2/20%H_2/N_2 flow at 40mL/min in different temperatures of 50 °C (black), 100 °C (red), 200 °C (blue), 300 °C (pink) at wavelength range of (a) 1200 to 1800 cm^{-1}, (b) 1825 to 2150 cm^{-1}, and (c) 2650 to 3150 cm^{-1}.

To observe the species formed during the CO_2 methanation reaction, *in situ* DRIFTS experiments were performed. **Figure 2** shows spectra taken at 50, 100, 200, and 300 °C in a flow of 10% CO_2/40% H_2/N_2 at 40 mL/min over the 5%Ru/Al_2O_3 catalyst. At 50 °C, prominent peaks at 1657, 1435, and 1228 cm^{-1} were observed, and these species are assigned to bicarbonate species.[31,37,40,41] This indicates that CO_2, in the presence of H_2, initially adsorbs on surface of 5%Ru/Al_2O_3 catalysts in the form of surface bicarbonate species at low temperatures. A band at 2002 cm^{-1} was also observed, indicating formation of linear carbonyl species.[42–44] At 100 °C, formation of new peaks at 1591, 1392, and 1374 cm^{-1}, along with small bands at 2996 and 2901

cm^{-1} were observed, indicating formate species were formed as the temperature increased to 100 °C.[45–47] The intensities of these peaks continued to increase as the temperature increased to 300 °C, implying that surface formate species become more prevalent on the catalyst surface as the temperature increases. On the other hand, the intensity of peaks indicating bicarbonate species decreased as the temperature increased, becoming completely unobservable by a temperature of 300 °C. This suggests that the bicarbonate species were either consumed as a reaction intermediate or were desorbed from the catalyst surface as the temperature increased. Similar to formate species, the intensity of the linear carbonyl peak increased with an increase in temperature. The peak at 2002 cm^{-1} also slightly shifted to 1997 cm^{-1} at 200 °C and 1991 cm^{-1} at 300 °C. This shift has been previously attributed to a decrease of dipole-dipole coupling owing to a decrease in surface coverage.[48] At 200 °C, a new peak at 3015 cm^{-1} was observed, indicating formation of methane. Overall, DRIFT spectra taken at different temperatures over 5% Ru/Al_2O_3 showed that bicarbonate, formate, and carbonyl species were observed during the CO_2 methanation reaction, and methane is likely formed by a reaction path that includes one or more of these observed species as reaction intermediates.

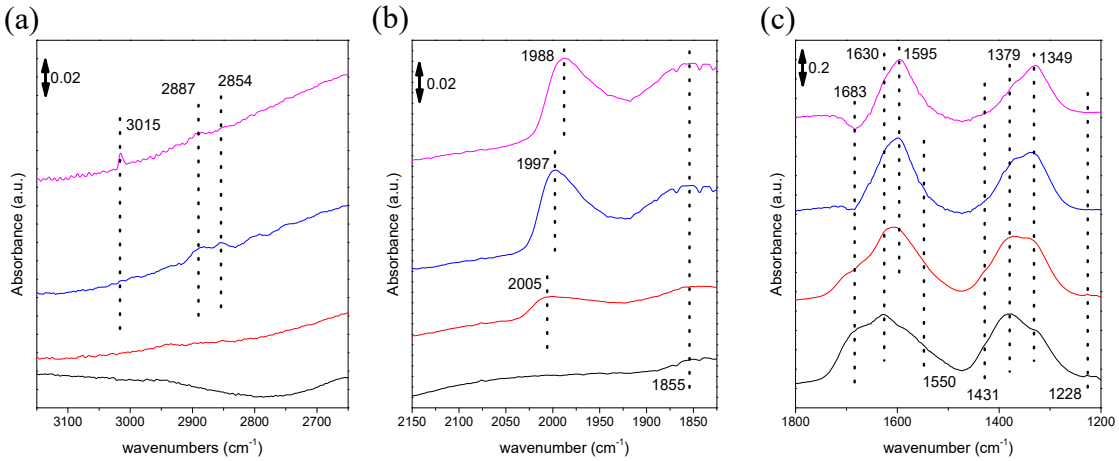

Figure 3. DRIFT spectra taken over $NaNO_3$/5% Ru/Al_2O_3 under 5%CO_2/20%H_2/N_2 flow at 40mL/min in different temperatures of 50 °C (black), 100 °C (red), 200 °C (blue), 300 °C (pink) at wavelength range of (a) 1200 to 1800 cm^{-1}, (b) 1825 to 2150 cm^{-1} and (c) 2650 to 3150 cm^{-1}.

Figure 3 shows IR spectra taken over $NaNO_3$/5% Ru/Al_2O_3 at various temperatures in a flow of 5% CO_2/20% H_2/N_2 at 40 mL/min. At 50 °C, wide bands centered at 1629 and 1379 cm^{-1}, along with shoulders at 1683, 1550, 1431, and 1330 cm^{-1}, were observed. Species observed at 1550 and 1379 cm^{-1} were assigned to monodentate carbonate, and those observed at 1630 cm^{-1} were assigned to bidentate carbonate.[49–51] A small peak observed at 1228 cm^{-1} along with the shoulder observed at 1431 cm^{-1} were assigned to bicarbonate species. A shoulder at 1683 cm^{-1} was assigned to CO_2^- species, as it was previously reported that the presence of alkali metal atoms decreases the work function of the surface, leading to charge transfer to an empty CO_2 π-orbital.[14,52,53] As the temperature increased to 100 °C, a new peak was formed at 1595 cm^{-1} and 1349 cm^{-1}, indicating formation of formate species, while the intensities of the peaks at 1379, 1550 and 1683 cm^{-1} decreased, implying the surface became more deficient in monodentate carbonate and CO_2 species. On the other hand, intensities of peaks at 1630 cm^{-1} became more intense as the temperature increased, which suggests that bidentate carbonate species became more prevalent with the temperature increase. A new peak at 2005 cm^{-1} was also formed, assigned to linear carbonyl species. Similar to what was observed over 5% Ru/Al_2O_3, a shift towards lower wavelengths was observed as the temperature increased. At 200 °C, additional two peaks were observed at 2887 and 2854 cm^{-1}, which are assigned to formate species. A small peak at 3015 cm^{-1} was observed as well, meaning methane formation started to occur at a temperature of 200 °C. Overall, the main difference in the spectra between the $NaNO_3$/5% Ru/Al_2O_3 and 5% Ru/Al_2O_3 catalysts was the presence of monodentate and bidentate carbonate species for $NaNO_3$ loaded samples at lower temperatures. While bicarbonate species were present in both catalysts, carbonate species showed

much higher peak intensities over the $NaNO_3$/5% Ru/Al_2O_3 catalyst, indicating carbonate species were more dominant over that catalyst surface than the bicarbonate species. Carbonyl species and formate species were observed on both catalysts as the temperature increased.

Similar DRIFT spectra were taken over 1%Ru/Al_2O_3 (**Figure S2**) and $NaNO_3$/1%Ru/Al_2O_3 (**Figure S3**) under 5% CO_2/20%H_2/N_2 at 40 mL/min at various reaction temperatures. Species observed on 1% Ru/Al_2O_3 were generally similar to those observed in 5% Ru/Al_2O_3, showing bicarbonate, formate, and carbonyl species. On the other hand, there were a few differences observed in the spectra of $NaNO_3$/1% Ru/Al_2O_3 and $NaNO_3$/5% Ru/Al_2O_3. For $NaNO_3$/1% Ru/Al_2O_3, there was a sharp peak observed at 1305 cm^{-1}. This peak is assigned to carboxylate species on the Al_2O_3 support.[43,54] While $NaNO_3$/5% Ru/Al_2O_3, did not show a prominent peak at 1305 cm^{-1}, it did show a wide shoulder ranging from 1320 to 1260 cm^{-1}, indicating that similar carboxylate species are present for $NaNO_3$/5%Ru/Al_2O_3 as well. It is likely that the carboxylate peak was less observable for $NaNO_3$/5% Ru/Al_2O_3 due to the more prominent bidentate carbonate peak. Another difference was that a wide band at 1855 cm^{-1} was observed over $NaNO_3$/5%Ru/Al_2O_3, while this band was not observed over $NaNO_3$/1%Ru/Al_2O_3. This band is assigned to bridged carbonyl species. In general, the intensity of carbonyl peaks was higher for the 5% Ru loading catalysts. Multiple previous works showed that bridged carbonyls typically are very low intensity bands.[37,38,43,44,46] Therefore, it is hypothesized that the bridged carbonyl species are most likely present in both $NaNO_3$/1%Ru/Al_2O_3 and $NaNO_3$/5%Ru/Al_2O_3 catalysts, but became more observable over the $NaNO_3$/5%Ru/Al_2O_3 catalyst, as the total exposed ruthenium surface area increased with higher metal loading, making various Ru-$(CO)_x$ species more detectable.

3.4. SSITKA/DRIFTs

While multiple surface species were observed through *in situ* DRIFTS experiments during the methanation reaction, reaction intermediates and spectator species cannot be distinguished by DRIFT spectra alone. To this end, isotopic transient experiments were performed over the previously tested four catalysts. Initially, a mixture of 5% $^{12}CO_2$/20% H_2/N_2 was flowed at 40 mL/min. Once steady-state conditions were reached in the IR spectra, the reactant was switched to $^{13}CO_2$/20%H_2/N_2 at same flow rate. The outlet of the IR cell was analyzed using a mass spectrometer to observe the transient response.

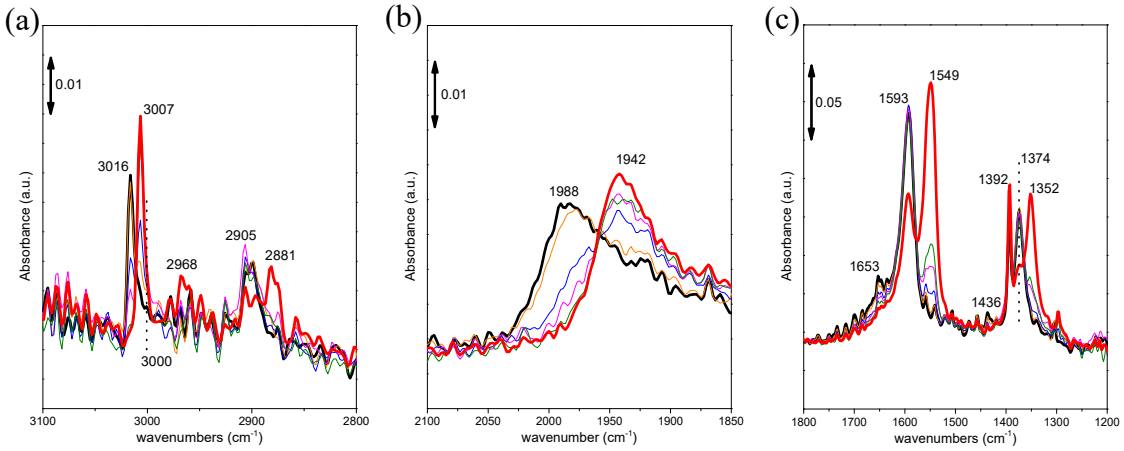

Figure 4. *In situ* DRIFT spectra taken over 5% Ru/Al_2O_3 catalysts at wavelength range of (a) 1200 cm^{-1} to 1800 cm^{-1}, (b) 1850 cm^{-1} to 2100 cm^{-1}, and (c) 2800 cm^{-1} to 3100 cm^{-1} at temperature of 260 °C under flow of 5% $^{12}CO_2$/20% H_2/N_2 (black, thickened) and after switch to 5% $^{13}CO_2$/20% H_2/N_2 flow. (28 s (orange), 56 s (blue), 85 s (pink), 113 s (green), and 8 min (red, thickened) after the switch).

Figure 4 shows the IR spectra after changing the flow from $^{12}CO_2/H_2$/He to $^{13}CO_2/H_2$/He at a temperature of 260 °C over 5% Ru/Al_2O_3. Initial peaks observed under $^{12}CO_2/H_2$/He flow were similar to those observed in **Figure 2**. Linear carbonyl species at 1988 cm^{-1}, formate species at 2905, 1593, 1392, and 1374 cm^{-1} were observed. Very small peaks at 1653 and 1436 cm^{-1} indicated that bicarbonate species are present as well. After switching the $^{12}CO_2$ feed to $^{13}CO_2$, the

linear $^{12}CO^*$ peak at 1988 cm^{-1} started to decrease immediately, while a new $^{13}CO^*$ peak was formed at 1942 cm^{-1}. The $^{12}CO^*$ peak became completely unobservable within 2 min. The formate species behaved very differently from the carbonyl species in that the $H^{12}COO^*$ peak at 1593 cm^{-1} showed a very slow decrease upon switching to $^{13}CO_2$. The intensity of the $H^{12}COO^*$ only decreased by 40% within 8 minutes after the switch. Furthermore, the formation of the $H^{13}COO^*$ peak at 1549 cm^{-1} was much slower than that of the $^{13}CO^*$, continuing to increase until 8 minutes after the switch. Changes in the normalized peak intensity observed in DRIFT spectra of the carbonyl and formate species are plotted as shown in **Figure 5** (a). As observed in the figure, the $^{12}CO^*$ and $H^{12}COO^*$ species decomposed at a very different rate, with $^{12}CO^*$ showing a decrease faster than the $H^{12}COO^*$ by an order of magnitude. Furthermore, the rate of decay observed for $^{12}CO^*$ peak was similar to the rate of decay observed for $^{12}CH_4$, as observed in **Figure 5** (b). The formation rate of $^{13}CO^*$ was also much faster than $H^{13}COO^*$, with the $^{13}CO^*$ species reaching a stable intensity within 150 s after the switch. Similarly, the $^{13}CH_4$ mass spectroscopy intensity also reached an equilibrium by 150 s. The observation that the decay of the $^{12}CO^*$ species occurred at similar rate to that of $^{12}CH_4$, as well as that formation of $^{13}CO^*$ species occurred at a similar rate as $^{13}CH_4$, suggests that the linear carbonyl species is a true reaction intermediate for the methanation reaction. In contrast, both the decay of $H^{12}COO^*$ and formation of $H^{13}COO^*$ occurred at very different rates to the rate of methane formation, indicating that formate species are most likely not significant reaction intermediates for the CO_2 methanation reaction over this catalyst. It is less clear whether the bicarbonate species are reaction intermediates using the spectra obtained over 5% Ru/Al_2O_3 because the intensity of the peaks at 1653 and 1436 cm^{-1} was very low, thereby making it difficult to perform the analysis done for CO and formate species.

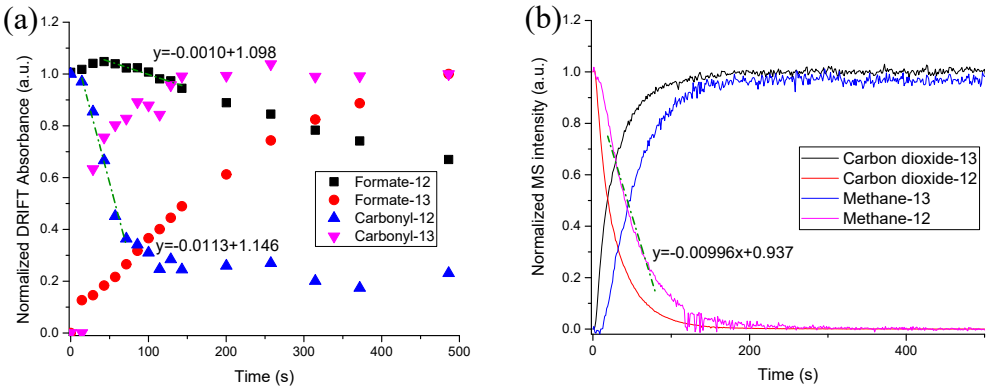

Figure 5. (a) Change in normalized DRIFT spectra intensity of observed surface species and (b) change in normalized mass spectroscopy intensity of $^{12}CO_2$, $^{13}CO_2$, $^{12}CH_4$, and $^{13}CH_4$, after switching from 5% $^{12}CO_2$/20% H_2/He flow to 5% $^{13}CO_2$/20% H_2/He flow over 5%Ru/Al_2O_3 catalysts at a temperature of 260 °C. Total flow rate was constant at 40 mL/min.

Similar transient isotopic experiments were performed over 1% Ru/Al_2O_3 as well, with **Figure S4** showing the IR spectra and **Figure S5** showing the normalized intensity of selected species observed in the IR spectra along with mass spectroscopy results. As observed in **Figure S5**, linear carbonyl and formate species showed similar trends as the 5% Ru/Al_2O_3 catalyst. Linear carbonyl species showed a rapid exchange between the ^{12}CO* (1996 cm^{-1}) and ^{13}CO* (1954 cm^{-1}) species after the switch. For the formate species, the decomposition of H^{12}COO* peaks was much slower than for 5%Ru/Al_2O_3. As observed in **Figure S4** (a), the peak in 2904 cm^{-1} showed an intensity change of less than 1 %, even after 8 min of flow with $^{13}CO_2$. In contrast, for the bicarbonate species (HCO_3), as observed with the peak at 1653 cm^{-1}, a rapid decomposition of H$^{12}CO_3$ species after the switch was observed. An increase in the peak at 1595 cm^{-1} along with formation of a shoulder at 1605 cm^{-1} were also observed after the switch. The peak at 1653 cm^{-1} represents O-^{12}C-O asymmetric stretching, and using Eq. (1), a peak shift to 1606 cm^{-1} is calculated for the same species with ^{13}C, which matches well with the shoulder formed.[46] Also, as mentioned

above, peaks indicating $H^{12}COO^*$ species showed very small changes in intensity, so it is unlikely the peak increase at 1595 cm^{-1} is representing an increase in $H^{12}COO^*$ coverage. Therefore, the increase in intensity of the 1595 cm^{-1} peak as well as formation of a shoulder at 1605 cm^{-1} are attributed to formation of $H^{13}CO_3$ after the switch. Under the assumption that the change in intensity of the 1595 cm^{-1} peak is essentially negligible, the changes in the normalized intensity for $H^{12}CO_3$ and $H^{13}CO_3$ species are plotted as shown in **Figure S5** (a). It should be noted that the IR intensity for $H^{12}COO^*$ was not plotted, as there was negligible change in its intensity. It was observed that the decomposition rates of the $^{12}CO^*$ and $H^{12}CO_3$ bands were very similar. Also, these rates were similar to the rate of decay for the $^{12}CH_4$ mass spectroscopy signal, as observed in **Figure S5** (b). Based on these observations, it is hypothesized that the linear carbonyl species and bicarbonate species are likely reaction intermediates for the CO_2 methanation reaction, while formate species are likely spectator species over the 1% Ru/Al_2O_3 catalysts. While a definitive statement cannot be made about the intermediacy of the bicarbonate species over 5%Ru/Al_2O_3 catalysts, based on the fact that similar behavior for carbonyl and formate species was observed, along with similar reaction orders for CO_2 and H_2 and activation energies for the two catalysts, it is likely that the bicarbonate species are reaction intermediates over the 5% Ru/Al_2O_3 catalyst as well.

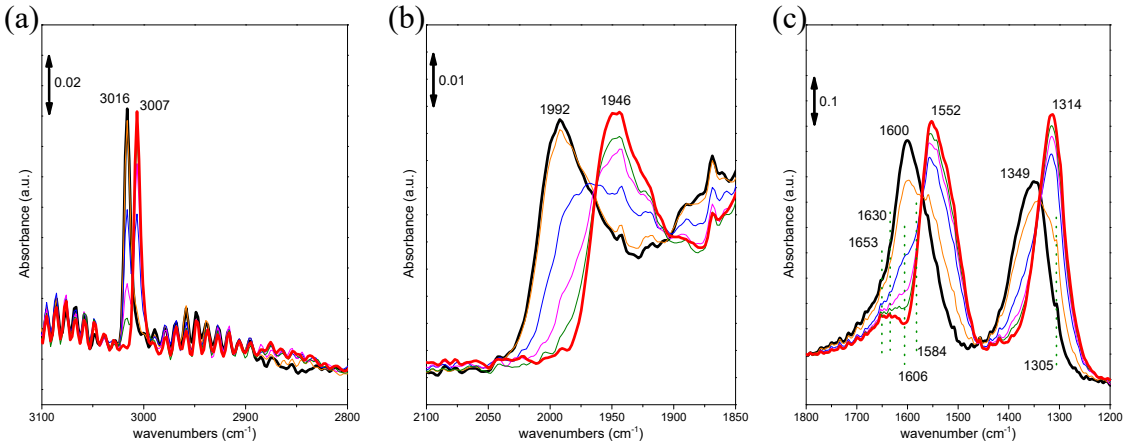

Figure 6. *In situ* DRIFT spectra taken over $NaNO_3$/5% Ru/Al_2O_3 catalysts at wavelength range of (a) 1200cm^{-1} to 1800cm^{-1}, (b) 1850 cm^{-1} to 2100 cm^{-1}, and (c) 2800 cm^{-1} to 3100 cm^{-1} at temperature of 260 °C under flow of 5% $^{12}CO_2$/20% H_2/N_2 (black, thickened) and after switch to 5% $^{13}CO_2$/20% H_2/N_2 flow. (28 s (orange), 56 s (blue), 85 s (pink), 113 s (green), and 8 min (red, thickened) after the switch).

Figure 6 shows IR spectra after changing the flow from $^{12}CO_2/H_2$/He to $^{13}CO_2/H_2$/He at a temperature of 260 °C over the $NaNO_3$/5% Ru/Al_2O_3 catalyst. Under $^{12}CO_2/H_2$/He flow, linear carbonyl species at 1992 cm^{-1}, formate species at 1600 cm^{-1} and 1348 cm^{-1}, bicarbonate species at 1653 cm^{-1}, bidentate carbonate species at 1630, and carboxylate species at 1305 cm^{-1} were observed. Similar to the unpromoted Ru/Al_2O_3 catalysts, linear carbonyl species showed a rapid exchange between ^{12}CO* and ^{13}CO* species, as observed in **Figure 6** (b). The peak at 1992 cm^{-1} decomposed quickly and became unobservable approximately 2 min after switching to $^{13}CO_2$ flow, and a new peak for ^{13}CO* was formed at 1946 cm^{-1}, which also reached a stable intensity over a similar interval. For bicarbonate species, while the intensity of the shoulder at 1653 cm^{-1} did decrease after the switch, the decrease in intensity was only by 37%, suggesting it is a relatively stable species that did not fully decompose, even 8 minutes after switching the feed to $^{13}CO_2$. Furthermore, if the bicarbonate species are reaction intermediates, a peak at 1606 cm^{-1}, with similar intensity as 1653 cm^{-1} in $^{12}CO_2$ flow should be observed after the switch. However, there was no band observed at 1606 cm^{-1} under $^{13}CO_2$ flow, which indicates that bicarbonate species are most

likely not a methanation reaction intermediate. The formate species showed a different trend from the Ru/Al_2O_3 catalysts. As observed in **Figure 6 (c)**, the intensities of peaks at 1600 cm^{-1} and 1349 cm^{-1} rapidly decreased upon switching to $^{13}CO_2$. Peaks at 1600 cm^{-1} and 1349 cm^{-1} represent symmetric and asymmetric O-C-O stretching of formate species, and therefore should form peaks at 1554 cm^{-1} and 1311 cm^{-1} upon switching to $^{13}CO_2$ according to Eq. (1). Such values correspond well to the rapidly formed peaks of 1552 cm^{-1} and 1314 cm^{-1} upon switch to $^{13}CO_2$. This observation implies that addition of $NaNO_3$ altered to some degree the reaction pathway(s) for CO_2 methanation, and formate species are likely also reaction intermediates for CO_2 methanation over $NaNO_3$/5% Ru/Al_2O_3. One thing to note is that the intensity of the newly formed peak at 1314 cm^{-1} was much larger than the initial 1349 cm^{-1} peak. This is attributed to presence of the carboxylate species observed at 1305 cm^{-1} as well. While a quick isotopic exchange for bidentate carbonate occurred, it is likely that the ^{12}C-carboxylate species were still present after the switch, making the newly formed bidentate $^{13}CO_3$ peak stack on the existing carboxylate peak, leading to the higher intensity observed at 1314 cm^{-1}.

The changes in normalized intensity of the carbonyl, formate, and bicarbonate peaks are plotted in **Figure 7 (a)**, and it can be observed that the decomposition of ^{12}CO and $H^{12}COO$ species showed similar rates to the decay rate of the $^{12}CH_4$ signal obtained from mass spectroscopy, as shown in **Figure 7 (b)**. The decomposition rate of $H^{12}CO_3$ species was clearly much slower than the decomposition of the other two species. While the differences in decomposition rates between the hypothesized reaction intermediate (carbonyl and formate) and spectator species (bicarbonate) were not as stark as in case of 5% Ru/Al_2O_3, where an order of magnitude difference was observed between the decomposition rate of carbonyl and formate species, this could be due, in part, to the fact that the peak in 1653 cm^{-1} had some overlap with both the carbonate peak at 1630 cm^{-1} and

the formate peak at 1600 cm^{-1}, making accurate quantification more challenging. The difference in decomposition rates combined with the stable band observed at 1653 cm^{-1}, even long after switching to $^{13}CO_2$, shows that the bicarbonate species are most likely not reaction intermediates.

The bidentate carbonate species observed at the 1631 cm^{-1} was more difficult to analyze than the other species, because carbonate bands are typically broad and this led to overlap between the $^{12}CO_3$ bands and $^{13}CO_3$ bands, making it difficult to establish a stable baseline before and after the isotopic switch. So, as a control experiment, a similar *in situ* DRIFT experiment was performed over $NaNO_3/Al_2O_3$ sample, as observed in **Figure S6**. It could be observed that the carbonate species formed are unstable and easily desorbed under He purge flow. However, in **Figure S6**, approximately 4~5 minutes were needed for the carbonate peak to reach a stable baseline in the helium purge flow, while in **Figure 6 (b)**, the shoulder at 1630 cm^{-1} reached the stable baseline after 2 minutes upon switching the flow to $^{13}CO_2$. The shorter time needed for carbonate peak decomposition in presence of H_2 indicates that the carbonate species, under methanation reaction conditions, is being consumed at a rate that is faster than desorption rate under helium purge, implying that the carbonate species may also be methanation reaction intermediates over $NaNO_3/Ru/Al_2O_3$ catalysts.

Also, the peak at 1630 cm^{-1} represents the asymmetric O-C-O stretching of $^{12}CO_3$, so using Eq. (1), a newly formed $^{13}CO_3$ should have a similar intensity at 1584 cm^{-1}.[51,55] As observed in **Figure 6** (c), a very similar IR intensity was observed between the shoulder at 1630 cm^{-1} under $^{12}CO_2$ flow and the new shoulder formed at 1584 cm^{-1} under $^{13}CO_2$, which corresponds well with the expected shift. Furthermore, it was observed from the isotopic exchange experiment that formate species are likely reaction intermediates over the 5% $NaNO_3$/5% Ru/Al_2O_3 catalysts. To form formate, it is reasonable to think that CO_2 would initially bind on the surface of the support

in form of carbonate, bicarbonate or carboxylate. However, observations from the isotopic exchange experiment indicated that bicarbonate or carboxylate species are unlikely to be reaction intermediates over $NaNO_3/Ru/Al_2O_3$ catalysts. Combining such reasoning and the correspondence of newly formed bidentate $^{13}CO_3$ peaks to the calculated shift, it was hypothesized that the carbonate species are true reaction intermediates over the 5% $NaNO_3$/5% Ru/Al_2O_3 catalysts.

Similar transient isotopic experiments were also performed over $NaNO_3$/1% Ru/Al_2O_3, as shown in **Figure S7** and **Figure S8**, and peak shapes along with peak shifts that occurred after switching to $^{13}CO_2$ were very similar to those observed for $NaNO_3$/5% Ru/Al_2O_3. Based on these observations, it was concluded that both catalysts most likely follow similar reaction pathways, which includes bidentate carbonate, formate, and linear carbonyl species as reaction intermediates in the path to methane.

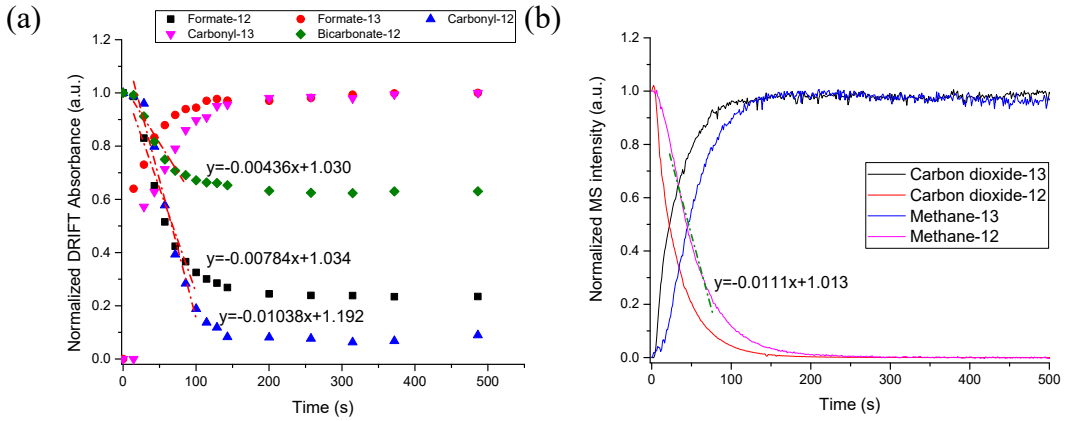

Figure 7. (a) Change in normalized DRIFT spectra intensity of observed surface species and (b) change in normalized mass spectroscopy intensity of $^{12}CO_2$, $^{13}CO_2$, $^{12}CH_4$, and $^{13}CH_4$, after switching from 5% $^{12}CO_2$/20% H_2/He flow to 5% $^{13}CO_2$/20% H_2/He flow over $NaNO_3$/5%Ru/Al_2O_3 catalysts at temperature of 260 °C. Total flow rate was constant at 40 mL/min.

3.5. Kinetic Modeling

Combining reaction orders calculated from kinetic measurements and spectral observations made from DRIFTS and SSITKA IR experiments, a sequence of reaction steps is proposed for methanation over Ru/Al_2O_3, as shown in **Table 2**. Since bicarbonate species, which were suggested as reaction intermediates from isotopic exchange experiments, are known to readily form on the surface of the alumina support, the interface between the metal and support is suggested to provide the reactive sites. For the Ru/Al_2O_3 catalyst, bicarbonate and linear carbonyl species were hypothesized to be reaction intermediates, while formate species were hypothesized to be spectator species. Thus, it is likely that CO_2 initially forms bicarbonate species, which eventually decomposes to form a linear carbonyl species, which then react with surface H* species to form methane. To this end, the initials steps of the proposed sequence over this catalyst includes the dissociation of H_2 into two H* atoms (**Table 2**, step 1), and the adsorption of CO_2 on hydroxyl groups on the metal-support interface to form bicarbonate species (**Table 2**, step 2). Then CO_2 adsorbed on the OH# site on the alumina surface transfers to the Ru metal site near the metal-support interface to form CO_2* (**Table 2**, step 3), which then reacts with H* to form CO* and OH* (**Table 2**, step 4). While CO_2* species were not observed in the FTIR spectra, it was hypothesized that such intermediate species are present, most likely in very low surface coverage, as it is unlikely for the linear carbonyl species to be formed from a bicarbonate species in a single elementary step. While formyl species (HCO*) could be another intermediate that may be in the reaction path from bicarbonate species to form CO*, it was conceptually hard to justify dissociating the C-H bond of HCO* to form CO* to then react with H* again to form CH*, so the formyl species was excluded from consideration as a potential reaction intermediate. As formate species (HCOO*) were also excluded as possible reaction intermediates from previous isotopic exchange analysis (**Figure 5**), it was hypothesized that the bicarbonate species decomposes to linear carbonyls through formation

of carboxylate (CO_2*) species on the Ru site. Numerous studies reported that the breaking of the C-O bond has the highest energy barrier over similar catalysts, and therefore the reaction of CO* with H* to break the carbonyl bond was taken as the rate determining step here.[56–60] The formed C* species are then hydrogenated to form the final product, methane.

Table 2. Proposed elementary step for CO_2 methanation over Ru/Al_2O_3 catalysts

Step	Reaction
1	$H_2(g) + 2* \leftrightarrow 2H*$
2	$CO_2(g) + OH\# \leftrightarrow HCO_3\#$
3	$HCO_3\# + * \leftrightarrow CO_2* + OH\#$
4	$CO_2* + H* \leftrightarrow CO* + OH*$
5 (RDS)	$CO* + H* \rightarrow C* + OH*$
6	$C* + H* \leftrightarrow CH* + *$
7	$CH* + H* \leftrightarrow CH_2* + *$
8	$CH_2+* + H* \leftrightarrow CH_3* + *$
9	$CH_3* + H* \leftrightarrow CH_4* + *$
10 (irreversible)	$OH* + H* \rightarrow H_2O* + *$
11	$CH_4* \leftrightarrow CH_4(g) + *$
12	$H_2O* \leftrightarrow H_2O(g) + *$

Assuming step 5 is the rate determining step, and all steps prior to step 5 are quasi-equilibrated, a rate law was derived as shown in Eq. (3). The derivation of Eq. (3) is shown in **Table S2**.

$$r = \frac{\sqrt{\left(k_5 k_{10} K_4 K_3 K_2 K_1^{\frac{3}{2}}\right)} P_{CO_2}^{\frac{1}{2}} P_{H_2}^{\frac{3}{4}}}{2} \Bigg/ \left(1 + \sqrt{K_1 P_{H_2}} + K_3 K_2 P_{CO_2} + \sqrt{K_4 K_3 K_2 K_1^{\frac{1}{2}}} P_{CO_2}^{\frac{1}{2}} P_{H_2}^{\frac{1}{4}} \left(\sqrt{\frac{k_{10}}{2k_5}} + \sqrt{\frac{2k_5}{k_{10}}}\right)\right)^2 \qquad \text{Eq. (3)}$$

Furthermore, experimental data obtained from **Figure 1** (a) and **Figure 1** (b) were fitted to the derived rate law (Eq. (3)) for the Ru/Al_2O_3 catalyst, as shown in **Figure 8**. Experimental data for both 1% Ru/Al_2O_3 and 5% Ru/Al_2O_3 fit the derived rate law well, showing a slope of nearly 1

for both samples with an R^2 value of 0.940 for 1% Ru/Al_2O_3 and 0.933 for 5% Ru/Al_2O_3. The average error between the calculated and experimental TOFs was 2.7 % for 1% Ru/Al_2O_3 and 3.6% for 5% Ru/Al_2O_3. The kinetic constants obtained from the kinetic modeling are presented in **Table 3**. Comparing the values obtained for k_5 and k_{10} in both catalysts, k_5 had values lower than k_{10} by at least an order of magnitude, implying that k_5 has higher energy barrier, further corroborating the assignment that step 5 is a RDS in the reaction. Calculated surface coverages of the reaction intermediates are shown in **Table S3** and **Table S4**. For both Ru/Al_2O_3 catalysts, surface coverages of the CO_2* intermediate were very low, which may be why an intermediate species between the bicarbonate and linear carbonyl species could not be observed in the IR spectra. The fact that CO* shows a high surface coverage aligns with the assumption that step 5 is the RDS.

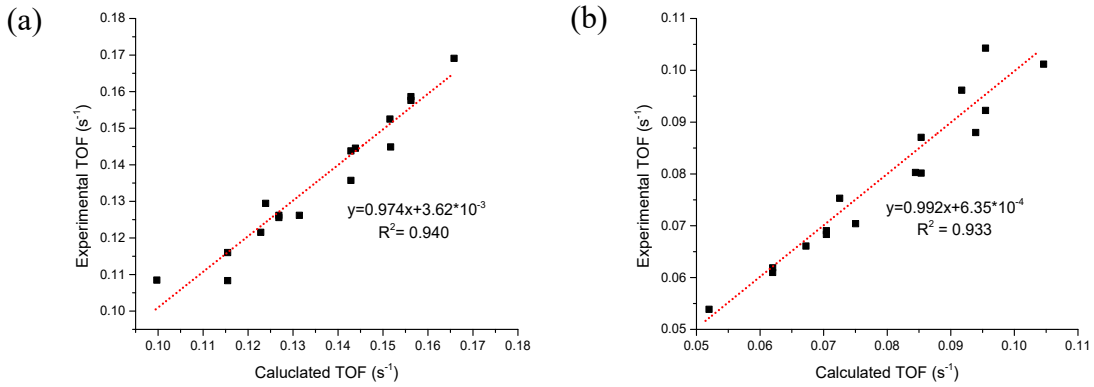

Figure 8. Calculated TOFs vs experimental TOFs for (a) 1% Ru/Al_2O_3 and (b) 5% Ru/Al_2O_3.

Table 3. Calculated kinetic constants for 1% Ru/Al_2O_3 and 5% Ru/Al_2O_3 catalysts at temperature of 260 °C.

Kinetic constants	1% Ru/Al_2O_3	5% Ru/Al_2O_3
K_1 (kPa^{-1})	0.0175 ± 0.00351	$2.25 \times 10^{-3} \pm 6.81 \times 10^{-4}$
$K_2 K_3$ (kPa^{-1})	$6.01 \times 10^{-6} \pm 2.97 \times 10^{-7}$	$6.37 \times 10^{-6} \pm 7.46 \times 10^{-7}$
K_4	121 ± 5.93	127 ± 14.7
k_5 (s^{-1})	1.43 ± 0.0976	1.78 ± 0.26
k_{10} (s^{-1})	187 ± 7.71	216 ± 25.9

For the $NaNO_3/Ru/Al_2O_3$ catalysts, a different reaction pathway was hypothesized, since the reaction intermediates determined from transient isotopic experiments were different from the unpromoted Ru/Al_2O_3 catalysts, and the CO_2 and H_2 reaction orders do not correspond to the rate law shown in Eq. (3). From previous activation energy measurements (**Figure 1** (e)), an increase in activation energy was observed upon addition of $NaNO_3$ to the Ru/Al_2O_3 catalysts, so it was hypothesized that a change in the RDS, or an addition of another irreversible step could play a role when $NaNO_3$ was added to the catalysts. Furthermore, the increased H_2 reaction order likely implied that the hydrogenation of an already hydrogenated product could be important in the rate determining step over $NaNO_3/Ru/Al_2O_3$ catalysts.[A] Previous DFT studies reported that while C-O bond breaking from carbonyl or formyl species has the highest energy barrier on supported Ru catalysts, thereby becoming rate determining step(s), it was also reported that hydrogenation of CH_3* to form methane is also a step that has a comparable energy barrier.[56,58,59] Duan et al. reported an energy barrier of 143 kJ/mol (1.48 ev) for reaction between formyl species and H* that leads to C-O bond breaking and 125 kJ/mol (1.30 ev) for reaction between CH_3* and H* to form CH_4*. Mushrif et al. also reported an activation barrier of 198 kJ/mol for reaction of CO* and H* to break C-O bonds, while 105 kJ/mol for CH_4* formation through reaction of CH_3* and H*. Combining

[A] Increased H_2 reaction order implies that more hydrogen atoms are involved in the transition state during the rate determining step than for the RDS of unpromoted Ru/Al_2O_3 catalysts.

our experimental observations with previously reported DFT studies, it was hypothesized that an additional kinetically relevant irreversible step of CH_3* and H* to form CH_4* may be important. A sequence of elementary and lumped steps for a reaction pathway that assumes two irreversible steps was developed for $NaNO_3/Ru/Al_2O_3$ catalysts, as shown in **Table 4**.

Table 4. Proposed elementary step for CO_2 methanation over $NaNO_3/Ru/Al_2O_3$ catalysts

Step	Reaction
1	$H_2(g) + 2* \leftrightarrow 2H*$
2	$CO_2(g) + O\# \leftrightarrow CO_3\#$
3	$CO_3\# + H* \leftrightarrow HCOO* + O\#$
4	$HCOO* + * \leftrightarrow CO* + OH*$
5 (irreversible)	$CO* + H* \rightarrow C* + OH*$
6	$C* + H* \leftrightarrow CH* + *$
7	$CH* + H* \leftrightarrow CH_2* + *$
8	$CH_2+* + H* \leftrightarrow CH_3* + *$
9 (irreversible)	$CH_3* + H* \rightarrow CH_4* + *$
10 (irreversible)	$OH* + H* \rightarrow H_2O* + *$
11	$CH_4* \leftrightarrow CH_4(g) + *$
12	$H_2O* \leftrightarrow H_2O(g) + *$

For $NaNO_3/Ru/Al_2O_3$ catalysts, carbonates and formate species, as well as carbonyl species were determined to be observable reaction intermediates. So, the initial hypothesized steps in the proposed sequence were dissociation of H_2 into two H* atoms (**Table 4**, step 1) and adsorption of CO_2 on an oxide group (or $NaNO_3$ melt) on the support near the support-metal interface, to form bidentate carbonate species (**Table 4**, step 2). Then, the bidentate carbonate species would react with surface hydrogen to form formate species (**Table 4**, step 3), followed by dissociation of the formate to form linear carbonyl species (**Table 4**, step 4). Then the carbonyl species react with a surface hydrogen to break the C-O bond, which was the first kinetically relevant step (**Table 4**, step 5). The formed C* is then hydrogenated to form CH_3* (**Table 4**, step 6~8), which then reacts

with additional surface hydrogen to form adsorbed methane (**Table 4**, step 9). This is the second kinetically relevant step in methane formation. Assuming step 9 is the rate determining step, a rate law was derived, as shown in Eq. (4). The derivation of Eq. (4) is shown in **Table S5**.

$$r = \frac{\sqrt{\left(\frac{k_5 k_{10} K_4 K_3 K_2 K_1^{\frac{3}{2}}}{2}\right)} P_{CO_2}^{\frac{1}{2}} P_{H_2}^{\frac{3}{4}}}{\left(1 + \sqrt{K_1 P_{H_2}}(1 + K_3 K_2 P_{CO_2}) + \sqrt{K_4 K_3 K_2 K_1^{\frac{1}{2}}} P_{CO_2}^{\frac{1}{2}} P_{H_2}^{\frac{1}{4}} \left(\sqrt{\frac{k_{10}}{2k_5}} + \sqrt{\frac{2k_5}{k_{10}}}\right) + \frac{P_{CO_2}^{\frac{1}{2}}}{k_9} \sqrt{\frac{k_5 k_{10} K_4 K_3 K_2}{2}} \left(\frac{P_{H_2}^{-\frac{5}{4}}}{K_1^{\frac{5}{4}} K_6 K_7 K_8} + \frac{P_{H_2}^{-\frac{3}{4}}}{K_1^{\frac{3}{4}} K_7 K_8} + \frac{P_{H_2}^{-\frac{1}{4}}}{K_1^{\frac{1}{4}} K_8} + K_1^{\frac{1}{4}} P_{H_2}^{\frac{1}{4}}\right)\right)^2}$$

Eq. (4)

Experimental data obtained from **Figure 1** (a) and **Figure 1** (b) were fit to the derived rate law (Eq. (4)) for the $NaNO_3/Ru/Al_2O_3$ catalyst, as shown in **Figure 9**. Experimental data for $NaNO_3$/1% Ru/Al_2O_3 and $NaNO_3$/5% Ru/Al_2O_3 fit the derived rate law well, showing a slope of nearly 1 for both samples with R^2 values of 0.978 and 0.987. The average error between calculated and experimental TOFs was 4.2 % for $NaNO_3$/1% Ru/Al_2O_3 and 3.6% for $NaNO_3$/5% Ru/Al_2O_3. The kinetic constants obtained from the kinetic modeling are presented in **Table 5**. Within each catalyst, among the three rate constants of k_5, k_9, and k_{10}, k_9 showed the lowest values, implying that step 9, the hydrogenation of CH_3*, may be the most kinetically significant step on the $NaNO_3$ loaded catalysts. k_5 was still smaller than k_{10}, implying that it is the second slowest step in this pathway to methane. The surface coverage of reaction intermediates calculated from the rate law are shown in **Table S6** and **Table S7**. The results show that for the catalysts of similar metal loading, the surface coverage of hydrogen decreased for the $NaNO_3$ loaded catalysts. This is conceptually consistent with experimental observations, as the much-increased H_2 reaction order implies that hydrogen is consumed at a faster rate, which would lead to decreased surface coverage. Additionally, in $NaNO_3$ loaded catalysts, CH_3* showed a very high surface coverage, while the surface coverage of CO* decreased compared to the values found for the Ru/Al_2O_3 catalysts.

Again, this supports the hypothesis that step 9 is the slowest step in the proposed reaction sequence. It has been previously reported that alkali metals strengthen the bond between the metal and carbon atom, while weakening the bond between the carbon atom and oxygen atom of carbon monoxide on the surface of a noble metal, which has been attributed to enhanced electron back-donation from the metal into the $2\pi^*$ antibonding orbital of CO, likely caused by electron transfer from the alkali metal to the valence band of the noble metal.[61,62] It is hypothesized that this property may have changed the RDS from the C-O dissociation step to hydrogenation of the CH_3* species. It should also be noted that the reaction pathway proposed in **Table 4** differs from the previously hypothesized reaction pathway over $NaNO_3/Ru/Al_2O_3$ catalysts from our previous work, as we previously hypothesized a hydrogen carbonyl species maybe involved in the rate determining step, which may be responsible for the increased hydrogen reaction order.[24] However, kinetic modeling was performed on the rate law (Eq.S14-15) derived for such reaction pathway (**Table S13**), and it was found that the surface coverage obtained from kinetic modeling does not correspond to the kinetic measurements. A higher hydrogen surface coverage was observed for $NaNO_3/Ru/Al_2O_3$ catalysts than Ru/Al_2O_3 catalysts, which does not align with the implication of the increased H_2 reaction order for the $NaNO_3$ promoted catalysts, which makes the hydrogen carbonyl pathway less likely to be the representative pathway. Further description the hydrogen carbonyl pathway, along with other reaction sequences considered for $NaNO_3/Ru/Al_2O_3$ catalysts, which were concluded to be less likely to be the representative pathways, are shown in the supplementary information (Section III).

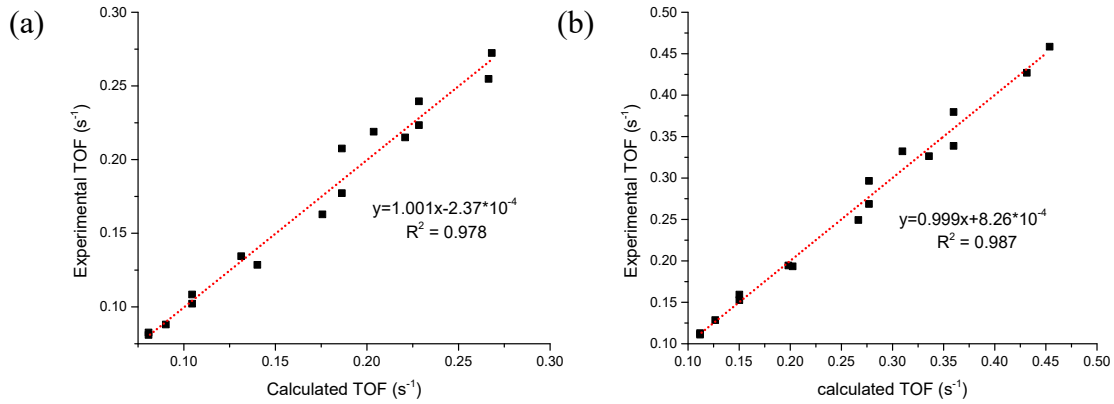

Figure 9. Calculated TOF vs experimental TOF for (a) $NaNO_3$/1% Ru/Al_2O_3 and (b) $NaNO_3$/5% Ru/Al_2O_3.

Table 5. Calculated kinetic constants for 1% Ru/Al_2O_3 and 5% Ru/Al_2O_3 catalysts at temperature of 260 °C.

Kinetic constants	$NaNO_3$/1% Ru/Al_2O_3	$NaNO_3$/5% Ru/Al_2O_3
K_1 (kPa^{-1})	54.1 ± 1.51	19.3 ± 0.202
K_2 K_3 (kPa^{-1})	$6.67 \times 10^{-6} \pm 6.00 \times 10^{-7}$	$1.12 \times 10^{-5} \pm 1.45 \times 10^{-6}$
K_4	26.7 ± 2.39	45.0 ± 5.68
k_5 (s^{-1})	120 ± 18.6	402 ± 37.8
K_6	$1.98 \times 10^{-5} \pm 3.83 \times 10^{-7}$	$3.30 \times 10^{-5} \pm 2.96 \times 10^{-7}$
K_7	$0.158 \pm 3.08 \times 10^{-3}$	$0.264 \pm 2.38 \times 10^{-3}$
K_8	7.87 ± 0.163	13.3 ± 0.127
k_9 (s^{-1})	1.83 ± 0.0911	4.30 ± 0.311
k_{10} (s^{-1})	3977 ± 349	4918 ± 494

4. Conclusions

To summarize, catalysts with different metal loadings (1% and 5%) on Ru/Al_2O_3 catalysts and $NaNO_3/Ru/Al_2O_3$ were synthesized, and their CO_2 methanation mechanisms were investigated. The former catalyst represents a prototypical CO_2 methanation catalyst, and the latter is a catalytic sorbent, with heavy $NaNO_3$ promotion driving high CO_2 sorption. Such materials might find use in reactive separations.[20–27] Through DRIFT spectroscopy, along with transient isotopic experiments, it was found that bicarbonate and linear carbonyl species behave as reaction intermediates in the path to methane over Ru/Al_2O_3 catalysts. For $NaNO_3/Ru/Al_2O_3$ catalysts,

bidentate carbonate, formate and linear carbonyl species appear to be reaction intermediates. Kinetic modeling showed that the C-O bond breaking of carbonyl species is a likely rate determining step for Ru/Al_2O_3, while there are likely more kinetically relevant steps, including the hydrogenation of CH_3* species to form methane, for the $NaNO_3/Ru/Al_2O_3$ catalyst. No significant differences in reaction pathways were observed between different metal loadings. This is likely due to the fact that the different metal loading catalysts maintained similar average particle sizes. The subtle differences in reaction pathways over $NaNO_3$ loaded supported ruthenium catalysts vs. the unpromoted catalysts gives insight into the kinetic consequences of catalyst designs targeting catalytic sorbents, where *in situ* CO_2 capture and subsequent conversion is targeted on a single solid material.

In considering these results, we also note several limitations of our study. First, while the carboxylate intermediate (CO_2*) was not observed from the spectral data, it was still assumed as a reaction intermediate in the proposed reaction pathways for unpromoted Ru/Al_2O_3. Bicarbonate and carbonyl species were the only species that were observed as reaction intermediates over unpromoted Ru/Al_2O_3 from spectral data. However, it is unlikely that carbonyl species are formed from bicarbonate species in a single elementary step. Therefore, several potential intermediates that may form between the bicarbonate or the carbonate and the carbonyl species were considered, including carboxylate (CO_2*), formyl (HCO*), and formate (HCOO*) species. Spectral observation showed that formate species are most likely spectator species over unpromoted Ru/Al_2O_3 catalysts and therefore were not considered as kinetically relevant intermediates. However, neither carboxylate nor formyl species were observed from the IR spectra. Between the two species, carboxylate species were chosen as the more plausible reaction intermediate, as it was hard to justify dissociating the C-H bond of HCO* to form CO* to then react with H* again to

form CH*. Thus, the lack of spectral observation for carboxylate or formyl species is a limitation of this study.

Another limitation is that the rate determining step was set primarily based on previously reported DFT literature. While selection of these RDSs is logical, and our experimental data showed an excellent fitting to the rate expression that was derived from selection of the specific RDS, Langmuir-Hinshelwood formalisms have some limitations in kinetically describing some reactions. Indeed, using the concept of degrees of rate control (DRC) in a microkinetic models can quantitatively show when multiple transition states are kinetically relevant, thereby enabling more rigorous selection of the RDSs.[63,64] Thus, while the proposed reaction sequences are shown to effectively reproduce of the kinetics of the reaction and therefore may represent a true reaction pathway based on our experimental data and kinetic data, other parallel paths may also occur. Lastly, an H_2 to D_2 isotopic exchange experiment could be performed as a future work, since it is proposed that there is a change in kinetically relevant step in volving H addition for the $NaNO_3$ promoted Ru catalysts. This and related experiments could also provide more information regarding the roles of bicarbonate and carbonate for $NaNO_3$ promoted catalysts.

5. Acknowledgement

This work was supported by the Center for Understanding and Control of Acid Gas-Induced Evolution of Materials for Energy (UNCAGE-ME), an Energy Frontier Research Center, funded by U.S. Department of Energy (US DoE), Office of Science, Basic Energy Sciences (BES) under Award DE-SC0012577. Fundamental structural characterization was performed at the Georgia Tech Institute for Electronics and Nanotechnology, a member of the National Nanotechnology Coordinated Infrastructure (NNCI), which is supported by the National Science Foundation

(ECCS-1542174). X. W. (SSITKA-IR effort) was supported by the U.S. Department of Energy, Office of Science, Office of Basic Energy Sciences, Chemical Sciences, Geosciences, and Biosciences Division, Catalysis Science program.

References

(1) Intergovernmental Panel on Climate Change. *Climate Change 2014 : Mitigation of Climate Change*; Cambridge University Press, 2014.

(2) Boden, T. A.; Marland, G.; Andres, R. J. Global, Regional, and National Fossil-Fuel CO_2 Emissions. Carbon Dioxide Information Analysis Center, Oak Ridge National Laboratory, U.S. Department of Energy. **2017**.

(3) World Energy Council. *World Energy Resources*; 2016.

(4) Wang, W.; Wang, S.; Ma, X.; Gong, J. Recent Advances in Catalytic Hydrogenation of Carbon Dioxide. *Chem. Soc. Rev.* **2011**, *40* (7), 3703–3727.

(5) Miao, B.; Ma, S. S. K.; Wang, X.; Su, H.; Chan, S. H. Catalysis Mechanisms of CO_2 and CO Methanation. *Catal. Sci. Technol.* **2016**, *6* (12), 4048–4058.

(6) Aziz, M. A. A.; Jalil, A. A.; Triwahyono, S.; Ahmad, A. CO_2 Methanation over Heterogeneous Catalysts: Recent Progress and Future Prospects. *Green Chem.* **2015**, *17* (5), 2647–2663.

(7) Wang, W.; Gong, J. Methanation of Carbon Dioxide: An Overview. *Front. Chem. Eng.* **2011**, *5* (1), 2–10.

(8) Frontera, P.; Macario, A.; Ferraro, M.; Antonucci, P. Supported Catalysts for CO_2 Methanation : A Review. **2017**, No. 1, 1–28.

(9) Lee, W. J.; Li, C.; Prajitno, H.; Yoo, J.; Patel, J.; Yang, Y.; Lim, S. Recent Trend in Thermal Catalytic Low Temperature CO_2 Methanation : A Critical Review. *Catal. Today* **2021**, *368* (February 2020), 2–19.

(10) Li, D.; Ichikuni, N.; Shimazu, S.; Uematsu, T. Hydrogenation of CO_2 over Sprayed Ru/TiO_2 Fine Particles and Strong Metal–Support Interaction. *Appl. Catal. A Gen.* **1999**, *180* (1–2),

227–235.

(11) Li, D.; Ichikuni, N.; Shimazu, S.; Uematsu, T. Catalytic Properties of Sprayed Ru/Al_2O_3 and Promoter Effects of Alkali Metals in CO_2 Hydrogenation. *Appl. Catal. A Gen.* **1998**, *172* (2), 351–358.

(12) Cimino, S.; Boccia, F.; Lisi, L. Effect of Alkali Promoters (Li, Na, K) on the Performance of Ru/Al_2O_3 Catalysts for CO_2 Capture and Hydrogenation to Methane. *J. CO_2 Util.* **2020**, *37*, 195–203.

(13) Petala, A.; Panagiotopoulou, P. Methanation of CO_2 over Alkali-Promoted Ru/TiO_2 Catalysts : I. Effect of Alkali Additives on Catalytic Activity and Selectivity. *Appl. Catal. B Environ.* **2018**, *224*, 919–927.

(14) Panagiotopoulou, P. Methanation of CO_2 over Alkali-Promoted Ru/TiO_2 Catalysts : II. Effect of Alkali Additives on the Reaction Pathway. *Appl. Catal. B Environ.* **2018**, *236*, 162–170.

(15) David, M.; Barrio, V. L.; Requies, M.; Cambra, J. F. Effect of the Addition of Alkaline Earth and Lanthanide Metals for the Modification of the Alumina Support in Ni and Ru Catalysts in CO_2 Methanation. *Catalysts* **2021**, *11*, 353.

(16) Liu, Q.; Wang, S.; Zhao, G.; Yang, H.; Yuan, M.; An, X.; Zhou, H.; Qiao, Y.; TianYuanyu. CO_2 Methanation over Ordered Mesoporous NiRu-Doped CaO-Al_2O_3 Nanocomposites with Enhanced Catalytic Performance. *Int. J. Hydrogen Energy* **2017**, *43* (1), 239–250.

(17) Tsiotsias, A. I.; Charisiou, N. D.; Yentekakis, I. V.; Goula, M. A. The Role of Alkali and Alkaline Earth Metals in the CO_2 Methanation Reaction and the Combined Capture and Methanation of CO_2. *Catalysits* **2020**, *10*, 812.

(18) Bermejo-López, A.; Pereda-Ayo, B.; González-Marcos, J. A.; González-Velasco, J. R.

Mechanism of the CO_2 Storage and in Situ Hydrogenation to CH_4. Temperature and Adsorbent Loading Effects over Ru-CaO/Al_2O_3 and Ru-Na_2CO_3/Al_2O_3 Catalysts. *Appl. Catal. B Environ.* **2019**, *256*, 117845.

(19) Porta, A.; Visconti, C. G.; Castoldi, L.; Matarrese, R.; Jeong-Potter, C.; Farrauto, R.; Lietti, L. Ru-Ba Synergistic Effect in Dual Functioning Materials for Cyclic CO_2 Capture and Methanation. *Appl. Catal. B Environ.* **2021**, *283* (July 2020), 119654.

(20) Duyar, M. S.; Treviño, M. A. A.; Farrauto, R. J. Dual Function Materials for CO_2 Capture and Conversion Using Renewable H2. *Appl. Catal. B Environ.* **2015**, *168–169*, 370–376.

(21) Wang, S.; Farrauto, R. J.; Karp, S.; Jeon, J. H.; Schrunk, E. T. Parametric , Cyclic Aging and Characterization Studies for CO_2 Capture from Flue Gas and Catalytic Conversion to Synthetic Natural Gas Using a Dual Functional Material (DFM). *J. CO_2 Util.* **2018**, *27*, 390–397.

(22) Duyar, M. S.; Ramachandran, A.; Wang, C.; Farrauto, R. J. Kinetics of CO_2 Methanation over Ru/γ-Al_2O_3 and Implications for Renewable Energy Storage Applications. *J. CO_2 Util.* **2015**, *12*, 27–33.

(23) Proaño, L.; Tello, E.; Arellano-Trevino, M. A.; Wang, S.; Farrauto, R. J.; Cobo, M. In-Situ DRIFTS Study of Two-Step CO_2 Capture and Catalytic Methanation over Ru, "Na_2O"/Al_2O_3 Dual Functional Material. *Appl. Surf. Sci.* **2019**, *479*, 25–30.

(24) Park, S. J.; Bukhovko, M. P.; Jones, C. W. Integrated Capture and Conversion of CO2 into Methane Using $NaNO_3$ /MgO + Ru/Al_2O_3 as a Catalytic Sorbent. *Chem. Eng. J.* **2021**, *420* (P3), 130369.

(25) Duyar, M. S.; Wang, S.; Arellano-Treviño, M. A.; Farrauto, R. J. CO_2 Utilization with a Novel Dual Function Material (DFM) for Capture and Catalytic Conversion to Synthetic

Natural Gas: An Update. *J. CO_2 Util.* **2016**, *15*, 65–71.

(26) Porta, A.; Matarrese, R.; Visconti, C. G.; Castoldi, L.; Lietti, L. Storage Material Effects on the Performance of Ru-Based CO_2 Capture and Methanation Dual Functioning Materials. *Ind. Eng. Chem. Res.* **2021**, *60*, 6706–6718.

(27) Jeong-potter, C.; Farrauto, R. Feasibility Study of Combining Direct Air Capture of CO_2 and Methanation at Isothermal Conditions with Dual Function Materials. *Appl. Catal. B Environ.* **2021**, *282*, 119416.

(28) Kowalczyk, Z.; Stolecki, K.; Rarog-Pilecka, W.; Miskiewicz, E.; Wilczkowska, E.; Karpinski, Z. Supported Ruthenium Catalysts for Selective Methanation of Carbon Oxides at Very Low CO_x/H_2 Ratios. *Appl. Catal. A Gen.* **2008**, *342*, 35–39.

(29) Truszkiewicz, E.; Zegadło, K.; Wojda, D.; Mierzwa, B.; Kepinski, L. The Effect of the Ruthenium Crystallite Size on the Activity of Ru/Carbon Systems in CO Methanation. *Top. Catal.* **2017**, *60* (17), 1299–1305.

(30) Berger, Y. G.; Rao, J. N.K. Adjusted jackknife for imputation under unequal probability sampling without replacement. *J. R. Stat. Soc. B*. **2006**, 68, 531-547.

(31) Wang, X.; Hong, Y.; Shi, H.; Szanyi, J. Kinetic Modeling and Transient DRIFTS–MS Studies of CO2 Methanation over Ru/Al_2O_3 Catalysts. *J. Catal.* **2016**, *343*, 185–195.

(32) Chukanov, N. V.; Chervonnyi, A. D. *IR Spectra of Minerals and Related Compounds, and Reference Samples ' Data*; Springer, 2016.

(33) Harada, T.; Hatton, T. A. Colloidal Nanoclusters of MgO Coated with Alkali Metal Nitrates/Nitrites for Rapid, High Capacity CO_2 Capture at Moderate Temperature. *Chem. Mater.* **2015**, *27*, 8153–8161.

(34) Zhang, K.; Li, X. S.; Li, W.; Rohatgi, A.; Duan, Y.; Singh, P.; Li, L.; King, D. L. Phase

Transfer-Catalyzed Fast CO_2 Absorption by MgO-Based Absorbents with High Cycling Capacity. *Adv. Mater. Interfaces* **2014**, *1*, 1400030.

(35) Park, S. J.; Kim, Y.; Jones, C. W. $NaNO_3$-Promoted Mesoporous MgO for High-Capacity CO_2 Capture from Simulated Flue Gas with Isothermal Regeneration. *ChemSusChem* **2020**, *13* (11), 2988–2995.

(36) Marwood, M.; Ralf, D.; Prairie, M.; Renken, A. Transient Drift Spectroscopy for the Determination of the Surface Reaction Kinetics of CO_2 Methanation. *Chem. Eng. Sci.* **1994**, *49* (24), 4801–4809.

(37) Karelovic, A.; Ruiz, P. Mechanistic Study of Low Temperature CO_2 Methanation over Rh/TiO_2 Catalysts. *J. Catal.* **2013**, *301*, 141–153.

(38) Wang, X.; Shi, H.; Kwak, J. H.; Szanyi, J. Mechanism of CO_2 Hydrogenation on Pd/Al_2O_3 Catalysts : Kinetics and Transient DRIFTS-MS Studies. *ACS Catal.* **2015**, *5*, 6337–6349.

(39) Marwood, M.; Doepper, R.; Renken, A. In-Situ Surface and Gas Phase Analysis for Kinetic Studies under Transient Conditions. The Catalytic Hydrogenation of CO_2. *Appl. Catal. A Gen.* **1997**, No. 151, 223–246.

(40) Morterra, C.; Magnacca, G. A Case Study : Surface Chemistry and Surface Structure of Catalytic Aluminas, as Studied by Vibrational Spectroscopy of Adsorbed Species. *Catal. Today* **1996**, *27*, 497–532.

(41) Solymosi, F.; Erdohelyi, A.; Kocsis, M. Methanation of CO_2, on Supported Ru Catalysts. *Faraday. Trans. 1* **1981**, *77*, 1003–1012.

(42) Gupta, N. M.; Kamble, V. S.; Iyer, R. M.; Ravindranathan, T.; Gratzel, M. The Transient Species Formed over $Ru\text{-}RuO_x/TiO_2$ Catalyst in the CO and CO + H_2 Interaction : FTIR Spectroscopic Study. *J. Catal.* **1992**, *486* (1992).

(43) Guo, Y.; Mei, S.; Yuan, K.; Wang, D.; Liu, H.; Yan, C.; Zhang, Y. Low-Temperature CO_2 Methanation over CeO_2-Supported Ru Single Atoms, Nanoclusters, and Nanoparticles Competitively Tuned by Strong Metal−Support Interactions and H - Spillover Effect. *ACS Catal.* **2018**, *8*, 6203–6215.

(44) Chin, S. Y.; Williams, C. T.; Amiridis, M. D. FTIR Studies of CO Adsorption on Al_2O_3- and SiO_2-Supported Ru Catalysts. *J. Phys. Chem. B* **2006**, *110*, 871–882.

(45) Erdohlyi, A.; Pasztor, M.; Solymosi, F. Catalytic Hydrogenation of CO_2 over Supported Palladium. *J. Catal.* **1986**, *98*, 166–177.

(46) Zhao, K.; Wang, L.; Calizzi, M.; Moioli, E.; Zu, A. In Situ Control of the Adsorption Species in CO_2 Hydrogenation : Determination of Intermediates and Byproducts. *J. Phys. Chem. C* **2018**, *122*, 20888–20893.

(47) Eckle, S.; Anfang, H.; Behm, R. J. Reaction Intermediates and Side Products in the Methanation of CO and CO_2 over Supported Ru Catalysts in H_2 -Rich Reformate Gases. *J. Phys. Chem. C* **2011**, *115* (4), 1361–1367.

(48) Alexeev, O. S.; Chin, S. Y.; Engelhard, M. H.; Ortiz-soto, L.; Amiridis, M. D. Effects of Reduction Temperature and Metal-Support Interactions on the Catalytic Activity of Pt/γ-Al_2O_3 and Pt/TiO_2 for the Oxidation of CO in the Presence and Absence of H_2. *J. Phys. Chem. B* **2005**, *109*, 23430–23443.

(49) Heyl, D.; Rodemerck, U.; Bentrup, U. Mechanistic Study of Low-Temperature CO_2 Hydrogenation over Modified Rh/Al_2O_3 Catalysts. *ACS Catal.* **2016**, *6*, 6275–6284.

(50) Wijnja, H.; Schulthess, C. P. ATR – FTIR and DRIFT Spectroscopy of Carbonate Species at the Aged γ-Al_2O_3/Water Interface. *Spectrochim. Acta. Part A* **1999**, *55*, 861–872.

(51) Du, H.; Williams, C. T.; Ebner, A. D.; Ritter, J. A. In Situ FTIR Spectroscopic Analysis of

Carbonate Transformations during Adsorption and Desorption of CO_2 in K-Promoted HTlc. *Chem. Mater.* **2010**, *22*, 3519–3526.

(52) Hoffmann, F. M.; Weisel, M. D.; Paul, J. The Activation of CO_2 by Potassium-Promoted Ru(001) I. FT-IRAS and TDMS Study of Oxalate and Carbonate Intermediates. *Surf. Sci.* **1994**, *316*, 277–293.

(53) Freund, H. J.; Roberts, M. W. Surface Chemistry of Carbon Dioxide. *Surf. Sci. Rep.* **1996**, *25*, 225–273.

(54) Li, C.; Sakata, Y.; Arai, T.; Domen, K.; Maruya, K.; Onishi, T. Carbon Monoxide and Carbon Dioxide Adsorption on Cerium Oxide Studied by Fourier- Transform Infrared Spectroscopy. *J. Chem. Soc., Faraday Trans. 1* **1989**, *85* (4), 929–943.

(55) Busca, G.; Lorenzelli, V. INFRARED SPECTROSCOPIC IDENTIFICATION OF SPECIES ARISING FROM REACTIVE ADSORPTION OF CARBON OXIDES ON METAL OXIDE SURFACES. *Mater. Chem.* **1982**, *7*, 89–126.

(56) Mohan, O.; Shambhawi, S.; Xu, R.; Lapkin, A. A.; Murshrif, S. H. Investigating CO_2 Methanation on Ni and Ru : DFT Assisted Microkinetic Analysis. *ChemCatChem* **2021**, 2420–2433.

(57) Schmider, D.; Maier, L.; Deutschmann, O. Reaction Kinetics of CO and CO_2 Methanation over Nickel. *Ind. Eng. Chem. Res.* **2021**, *60*, 5792–5805.

(58) Akamaru, S.; Shimazaki, T.; Kubo, M.; Abe, T. Density Functional Theory Analysis of Methanation Reaction of CO_2 on Ru Nanoparticle Supported on TiO_2 (101). *Appl. Catal. A Gen.* **2014**, *470*, 405–411.

(59) Zhang, S.; Yan, H.; Wei, M.; Evans, D. G.; Duan, X. Hydrogenation Mechanism of Carbon Dioxide and Carbon Monoxide on Ru(0001) Surface : A Density Functional Theory Study.

RSC Adv. **2014**, *4*, 30241–30249.

(60) Avanesian, T.; Gusmão, G. S.; Christopher, P. Mechanism of CO_2 Reduction by H_2 on Ru(0001) and General Selectivity Descriptors for Late-Transition Metal Catalysts. *J. Catal.* **2016**, *343*, 86–96.

(61) Garfunkel, E. L.; Crowell, J. E.; Somorjai, G. A. The Strong Influence of Potassium on the Adsorption of CO on Platinum Surfaces. A Thermal Desorption Spectroscopy and High-Resolution Electron Energy Loss Spectroscopy Study. *J. Phys Chem*. **1982**, *86*, 310–313.

(62) Pazmino, J. H.; Shekhar, M.; Williams, W. D.; Akatay, M. C.; Miller, J. T.; Delgass, N. W.; Ribeiro, F. H. Metallic Pt as active sites for the water–gas shift reaction on alkali-promoted supported catalysts. *J. Catal*. **2012**, *286*, 279–286.

(63) Campbell, C. T. The Degree of Rate Control : A Powerful Tool for Catalysis Research. *ACS Catalysis*. **2017**, *7*, 2770–2779.

(64) Foley, B. L.; Bhan, A. Degrees of Rate Control at Non(pseudo)steady-State Conditions. *ACS Catalysis*. **2020**, *10*, 2556–2564